


Article

Controllable Preparation to Boost High Performance of Nanotubular SiO₂@C as Anode Materials for Lithium-Ion Batteries

Chaoyun Shi ¹, Jingbo Chen ^{1,2,*} , Tong Guo ³, Guiyang Luo ³, Huili Shi ¹, Zixu Shi ¹, Guoqiang Qin ¹, Long Zhang ¹ and Xiangming He ^{4,*} 

¹ College of Chemistry and Chemical Engineering, Guizhou University, Guiyang 550025, China

² Collaborative Innovation Center of Guizhou Province for Efficient Utilization of Phosphorus and Fluorine Resources, Guizhou University, Guiyang 550025, China

³ College of Material and Metallurgy, Guizhou University, Guiyang 550025, China

⁴ Institute Nuclear & New Energy Technology, Tsinghua University, Beijing 100084, China

* Correspondence: jbchen@gzu.edu.cn (J.C.); hexm@tsinghua.edu.cn (X.H.)

Abstract: Due to poor electrical conductivity and significant volume change during the lithiation/delithiation process, the application of silica anode materials for lithium-ion batteries is severely limited. Here, SiO₂ nanotubes with a uniform and complete carbon layer were prepared employing ZnO nanorods as templates. The controllable wall thickness of SiO₂ nanotubes is about 11 nm, and the thinner wall reduces the lithium-ion diffusion distance and boosts performance. The uniform and complete carbon layer leads to a perfect dispersity of SiO₂ nanotubes, enhances the overall electrical conductivity, and also buffers the mechanical stresses caused by volume change, which helps to exhibit high specific capacity and a long cycle life. The nanotubular SiO₂@C composite reveals a high discharge specific capacity of about 526.3 mAh g⁻¹ at a current density of 1 A g⁻¹ after 500 cycles without significant capacity fade. In addition, it demonstrates excellent rate performance, which can maintain above 420 mAh g⁻¹ even at a current density of 5 A g⁻¹. The strategy may be adopted to prepare other anode materials as well.

Keywords: lithium-ion batteries; anode materials; SiO₂ nanotubes; SiO₂@C



Citation: Shi, C.; Chen, J.; Guo, T.; Luo, G.; Shi, H.; Shi, Z.; Qin, G.; Zhang, L.; He, X. Controllable Preparation to Boost High Performance of Nanotubular SiO₂@C as Anode Materials for Lithium-Ion Batteries. *Batteries* **2023**, *9*, 107. <https://doi.org/10.3390/batteries9020107>

Academic Editor: Hirotoishi Yamada

Received: 15 November 2022

Revised: 31 January 2023

Accepted: 1 February 2023

Published: 3 February 2023



Copyright: © 2023 by the authors. Licensee MDPI, Basel, Switzerland. This article is an open access article distributed under the terms and conditions of the Creative Commons Attribution (CC BY) license (<https://creativecommons.org/licenses/by/4.0/>).

1. Introduction

Because of their high power density, extended cycle life, favorable safety, and environmental friendliness, lithium-ion batteries (LIBs) have inspired tremendous interest as energy storage systems for electric vehicles, portable electronic devices, stationary storage, and so on [1–5]. With the development of technology, LIBs with higher power density, better cycle stability, and longer service life are required. The anode material is a key part that determines the electrochemical properties of LIBs. In order to satisfy the increasing requirement for LIBs with high energy density, many electrochemically active materials with high theoretical specific capacity have been proposed to replace commercial graphite, which has a theoretical capacity of only 372 mAh g⁻¹.

Due to high theoretical capacity (1965 mAh g⁻¹), great safety, and rich resources, SiO₂ has been considered to be the most promising alternative material for the next generation of LIBs [6,7]. However, in addition to low electronic conductivity, SiO₂ has a significant volume change during the lithiation/delithiation process, resulting in poor electrochemical performance [8–11]. It severely restricts the application of SiO₂ as an anode material for LIBs.

Some researchers have used some strategies such as structural design and composite material design to alleviate the volume expansion and enhance the poor electrical conductivity [12–14]. In terms of structural design, SiO₂ anode materials are prepared into

unique morphologies such as nanospheres [15,16], nanowires [17], nanotubes [18], and porous structures [19,20] to optimize electronic and lithium-ion (Li^+) diffusion channels. With regard to composite materials design, coating carbon is one of the most popular methods because of good electrical conductivity and the small volume expansion of carbon [21]. Compared to pure SiO_2 materials, the SiO_2 /carbon composite materials show higher electrical conductivity [22], and the carbon coating layer acts as a buffer medium, preventing mechanical stress induced by large volume variation, which leads to the formation of stable solid electrolyte interphase (SEI) films and improves the electrochemical performance [23]. Shi et al. [24] studied silica/carbon nanocomposites with a specific capacity of 434 mAh g^{-1} over 50 cycles at a current density of 100 mA g^{-1} utilizing heat and acid treatments. Guo et al. [25] demonstrated a hydrothermal-reaction-based silica nanoparticle/hard carbon composite with a specific capacity of 600 mAh g^{-1} over 12 cycles. Wang [26] et al. prepared graphene-coated silica nanotube networks (SiO_2 -NT/G networks), which had good electrochemical performances at a current density of 0.1 A g^{-1} . Gao [27] et al. prepared MHSiO_2 @C nanocomposites by chemical polymerization within the shell of MHSiO_2 using polydopamine (PDA) as the carbon source. The continuous carbon layer improved the electronic conductivity and structural stability of MHSiO_2 @C. At a current density of 0.5 mA g^{-1} , the reversible capacity of MHSiO_2 @C was as high as 440.7 mAh g^{-1} after 500 cycles.

Due to the high aspect ratio, SiO_2 nanotube anode material and electrolytes have a large contact surface area, which reduces Li^+ diffusion length. In addition, the enormous volume change is alleviated by hollow structures [28]. Therefore, a good electrochemical performance is demonstrated. The main methods used to prepare SiO_2 nanotubes are CVD [18], electrospinning [29,30], the template method [26,31,32], and so on. Using zinc oxide as a template, there are few papers on the synthesis of silica nanotubes for anode materials, as far as we know. Compared to other conventional templates, ZnO is cheap and simple to synthesize, and it can be easily dissolved in mild acid or base solutions, thus removal would be simple. Moreover, unfortunately so far the cycle performance of silica-based anode materials at high current density has been little studied, which is very important for industrial applications.

In this paper, ZnO nanorods as templates, glucose as carbon sources, and TEOS were used to prepare nanotubular carbon-coated SiO_2 (SiO_2 @C) composites with controllable wall thickness by a template method. The composite has an outstanding electrochemical performance, especially a long cycle life even at high current density. It is reasonable to assume that SiO_2 @C composites will meet the requirements of industrial application.

2. Materials and Methods

2.1. Chemicals and Reagents

For the synthesis of SiO_2 @C composites, the following reagents were used: zinc acetate ($(\text{CH}_3\text{COO})_2\text{Zn}$, AR), potassium hydroxide (KOH, AR), zinc nitrate ($\text{Zn}(\text{NO}_3)_2 \cdot 6\text{H}_2\text{O}$, AR, purity $\geq 99\%$), hexamethylenetetramine (HMT, AR), anhydrous ethanol (AR), tetraethoxysilane (TEOS), hydrochloric acid (HCl, AR, 38 wt%), ammonium hydroxide ($\text{NH}_3 \cdot \text{H}_2\text{O}$, AR), and isopropanol (AR, purity $\geq 99.7\%$). All above-mentioned chemicals and reagents were obtained from Shanghai Sinopharm Chemical Reagent Co., Ltd., China. Glucose (AR) was purchased from TianJin Yongda Chemical Reagent Co., Ltd., China. For the cell assembly, acetylene black (AR) and sodium alginate (AR) were purchased from Shanghai Macklin Chemical Reagent Co., Ltd., China. All chemical reagents used in this work were not further purified.

2.2. Fabrication of Nanotubular SiO_2 @C Composites

Scheme 1 shows the preparation process of nanotubular SiO_2 @C composites. First, zinc oxide nanorods were prepared. $\text{Zn}(\text{NO}_3)_2 \cdot 6\text{H}_2\text{O}$ (8.01 g) and HMT (1.89 g) were mixed in deionized water (DI water, 400 mL) and dispersed ultrasonically, and the solution was heated to 60°C . $(\text{CH}_3\text{COO})_2\text{Zn}$ (0.54 g) and KOH (0.42 g) were ultrasonically dispersed in

130 mL and 120 mL of anhydrous ethanol, respectively. Then, $(\text{CH}_3\text{COO})_2\text{Zn}$ solution and KOH solution were mixed thoroughly at room temperature. An amount of 45 mL of mixed solution was added to the above solution containing $\text{Zn}(\text{NO}_3)_2 \cdot 6\text{H}_2\text{O}$ and HMT, further heated to 90°C and mechanically stirred for 10 h. ZnO nanorods were prepared after being filtered and dried.



Scheme 1. Synthesis illustration of the nanotubular $\text{SiO}_2@\text{C}$ composites.

ZnO nanorods were added in the mixed solution containing isopropyl alcohol (120 mL), DI water (16 mL), and $\text{NH}_3 \cdot \text{H}_2\text{O}$ (4 mL). After the solution was mechanically stirred at room temperature, TEOS (2.4 mL) was added drop-wise. Centrifugation was used to gather $\text{ZnO}@\text{SiO}_2$ nanorods, which were then washed and dried. The obtained $\text{ZnO}@\text{SiO}_2$ nanorods were named as $\text{ZnO}@\text{SiO}_2$ -1, $\text{ZnO}@\text{SiO}_2$ -2, and $\text{ZnO}@\text{SiO}_2$ -3 according to the reaction times, which were 1 h, 2 h, and 3 h, respectively. $\text{ZnO}@\text{SiO}_2$ nanorods were added in 1 M HCl solution to remove the ZnO template, and SiO_2 nanotubes were obtained. The prepared SiO_2 nanotubes were named as SiO_2 -1, SiO_2 -2, and SiO_2 -3 according to the reaction time.

Nanotubular $\text{SiO}_2@\text{C}$ composites were prepared with SiO_2 nanotubes as reactants. SiO_2 nanotubes and glucose were added in anhydrous ethanol, stirred for 3 h to disperse well, and dried by stirring in an oil bath at 90°C to obtain $\text{SiO}_2@\text{glucose}$. Then, $\text{SiO}_2@\text{glucose}$ was placed in an argon atmosphere and heated up to 800°C for 3 h. Finally, nanotubular $\text{SiO}_2@\text{C}$ composites were prepared and named as $\text{SiO}_2@\text{C}$ -1, $\text{SiO}_2@\text{C}$ -2, and $\text{SiO}_2@\text{C}$ -3 according to the different mass ratios (1:1, 1:2, and 1:3, respectively) of SiO_2 nanotubes and glucose.

2.3. Characterizations

The crystallographic information of the prepared sample was measured using a powder X-ray diffractometer (XRD, D8 advance, Germany) at a scan speed of 5° min^{-1} in an angle range of $5\text{--}90^\circ$. Transmission electron microscopy (TEM, Tecnai G2 F20, USA) and scanning electron microscopy (SEM, JEOL 6300/7001, Japan) were applied to check the morphology of the sample. The carbon content was obtained via thermogravimetric analysis (TG, TG 209 F1 Libra, Germany) at a rate of $10^\circ\text{C min}^{-1}$ at a temperature range of $20\text{--}800^\circ\text{C}$. The functional groups of the sample were characterized by Fourier transform infrared spectroscopy (FTIR, Nicolet iS50, USA). Raman spectroscopy (Raman, LabRAM HR Evolution, France) was measured to analyze the defect and disordered structure of carbon in the composite. All samples were excited with 532 nm visible light and tested in a range of $100\text{--}3500 \text{ cm}^{-1}$. The chemical bonding and the chemical state of the prepared sample were determined by X-ray photoelectron spectroscopy (XPS, K-Alpha Plus, USA) with an Al $\text{K}\alpha$ radiation source.

2.4. Electrochemical Measurements

By assembling CR2032 coin-type cells in a glove box filled with Ar, electrochemical analysis was tested. The separator was Celgard 2400 (polypropylene), the anode was lithium, the binder was sodium alginate, and the conductive agent was acetylene black in this paper. The electrode slurry was uniformly coated on the copper foil using DI water as a

solvent, and the copper foil coated with active materials was dried at 110 °C for 12 h under vacuum. The diameter of the prepared electrode was 12 mm and the area loading mass of the active materials was about 0.26–0.41 mg cm^{−2}. LiPF₆ (1 mol L^{−1}) was dissolved into a mixed solution of ethylene carbonate (EC), diethyl carbonate (DEC), and ethyl methyl carbonate (EMC) with a volume ratio of 1:1:1, which was used as the electrolyte. By using a Land battery test system, the charge and discharge tests were executed in a potential range of 0.01–3.0 V. In a frequency range of 1.0×10^{-2} – 1.0×10^5 Hz, electrochemical impedance spectroscopy (EIS) experiments were performed on a CHI660A electrochemical workstation using fresh coin-type cells. At a scan rate of 0.1 mV s^{−1}, cyclic voltammetry (CV) was conducted in a potential range of 0.01–3.0 V.

3. Results and Discussion

3.1. Structure and Morphology Analysis

To demonstrate microscopic morphology, SEM and TEM tests were performed. Figure 1a–c display SEM images of ZnO@SiO₂; Figure 1d–f exhibit SEM images of SiO₂; and Figure 1g–i illustrate SEM images of SiO₂@C. SEM images demonstrate that SiO₂ has a regular tubular structure with homogeneous morphology, and the removal of the ZnO template and carbon coating layer has no impact on the shape. There is obviously a perfect dispersity of SiO₂ nanotubes. In addition, the wall thickness of SiO₂ nanotubes increases with the increase in reaction times, which further demonstrates that reaction times can be changed to regulate the wall thickness of SiO₂ nanotubes.

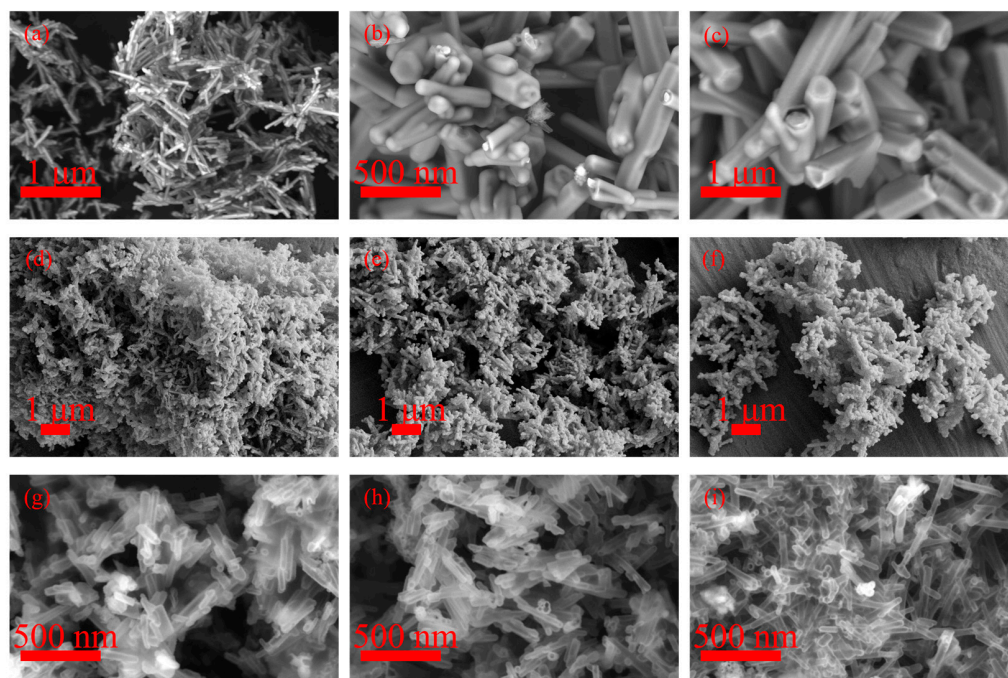


Figure 1. SEM images of (a) ZnO@SiO₂-1, (b) ZnO@SiO₂-2, (c) ZnO@SiO₂-3, (d) SiO₂-1, (e) SiO₂-2, (f) SiO₂-3, (g) SiO₂@C-1, (h) SiO₂@C-2, (i) SiO₂@C-3.

Figure 2 shows TEM images of SiO₂ nanotubes with different reaction times. The TEM images clearly show that the prepared SiO₂ has a uniform tubular morphology and nanotube walls are all relatively thin [26,32]. As can be observed, the wall thickness of SiO₂ nanotubes is around 11 nm, 23 nm, and 30 nm at reaction times of 1 h, 2 h, and 3 h, respectively. It illustrates that the wall thickness of SiO₂ nanotubes can be adjusted by controlling the reaction time of hydrolysis and polycondensation of TEOS, and the wall thickness increases with the reaction time. Therefore, the wall thickness of SiO₂ nanotubes will be further reduced by controlling the reaction time.

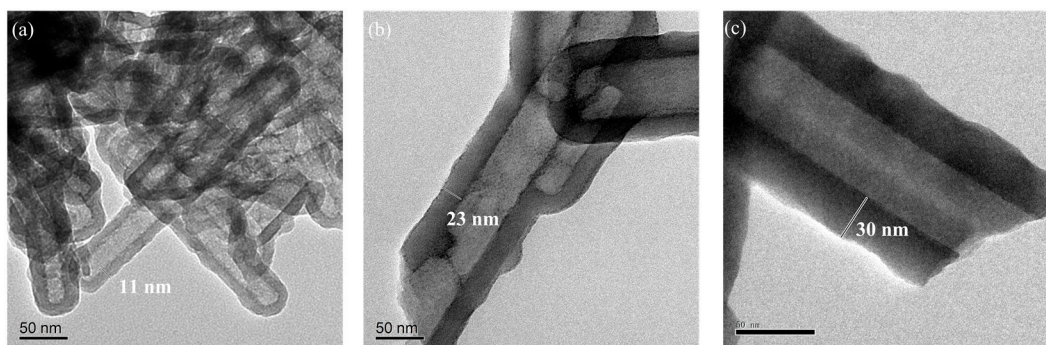


Figure 2. TEM images of (a) SiO₂-1, (b) SiO₂-2, (c) SiO₂-3.

XRD patterns are illustrated in Figure 3a. As can be observed, there are distinct wide peaks at $2\theta = 23^\circ$, indicating that SiO₂@C composites and SiO₂ are amorphous.

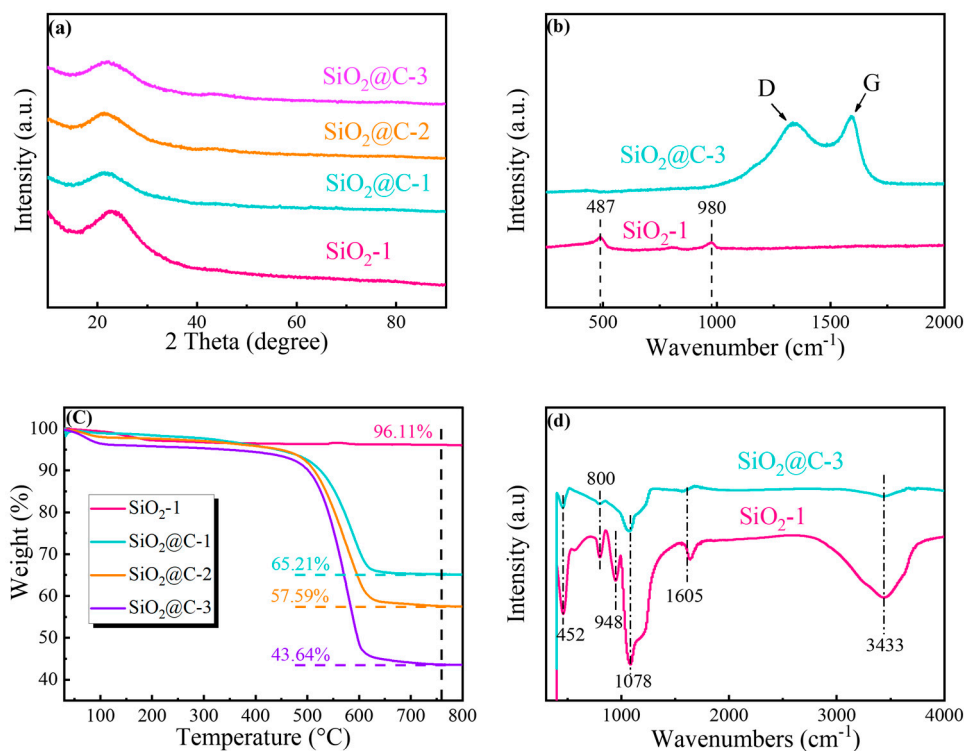


Figure 3. (a) XRD patterns of SiO₂ and SiO₂@C composites, (b) Raman spectra of SiO₂ and SiO₂@C-3 composites, (c) TG curves of SiO₂ and SiO₂@C composites, (d) FTIR spectra of SiO₂ and SiO₂@C-3 composites.

Raman spectra (Figure 3b) demonstrate the presence of carbon in SiO₂@C-3 composites. The two peaks of SiO₂@C-3 composites situated at 1337 cm⁻¹ and 1593 cm⁻¹ are corresponding to the D-band associated with carbon atoms with dangling bonds and the G-band associated with the vibration of carbon atoms with sp² hybridization, respectively [33]. In addition, carbon has a high degree of graphitization, since the strength of the G-band is greater than that of the D-band [27]. Additionally, SiO₂ can be identified by two peaks at 487 cm⁻¹ and 980 cm⁻¹. In Raman spectra of SiO₂@C-3, because the carbon layer is too thick and the carbon completely coats the SiO₂, the Raman information of SiO₂ may not be detected and peaks of SiO₂ cannot be observed [27].

To investigate the carbon content, TG tests were performed. Figure 3c displays TG curves. The weight of the SiO₂@C composites sharply drops from 500 °C to 600 °C, which is primarily attributed to the gasification of amorphous carbon. Therefore, it can be calculated

that the carbon contents of SiO₂@C-1, SiO₂@C-2, and SiO₂@C-3 composites are 30.9%, 38.52%, and 50.33%, respectively.

Functional groups of materials were identified to further explore the structure by FT-IR and are displayed in Figure 3d. In the FT-IR spectrum, the peaks located at 1078 cm⁻¹, 800 cm⁻¹, and 452 cm⁻¹ are corresponding to the asymmetric stretching, symmetric stretching, and bending vibrations of Si–O–Si [34,35]. Bands at 3433 cm⁻¹ and 948 cm⁻¹ are corresponding to the O–H and Si–O stretching vibration of Si–OH, respectively [36].

The XPS spectrum proves chemical states of Si, C, and O elements in SiO₂@C-3 composites. In Figure 4a, there are characteristic peaks of Si 2p, C 1s, and O 1s, indicating that the SiO₂@C-3 composite is thought to contain Si, C, and O elements. A characteristic peak corresponding to Si⁴⁺ (103.5 eV) can be noticed in Si 2p spectrum (Figure 4b) [37,38], indicating that the Si element exists in the form of SiO₂. The C 1s spectrum can be seen in Figure 4c, and after being fitted, three peaks occur at 284.1 eV, 285.1 eV, and 288.8 eV. The three peaks are corresponding to C–C, C–O and C=O bonds, respectively [39].

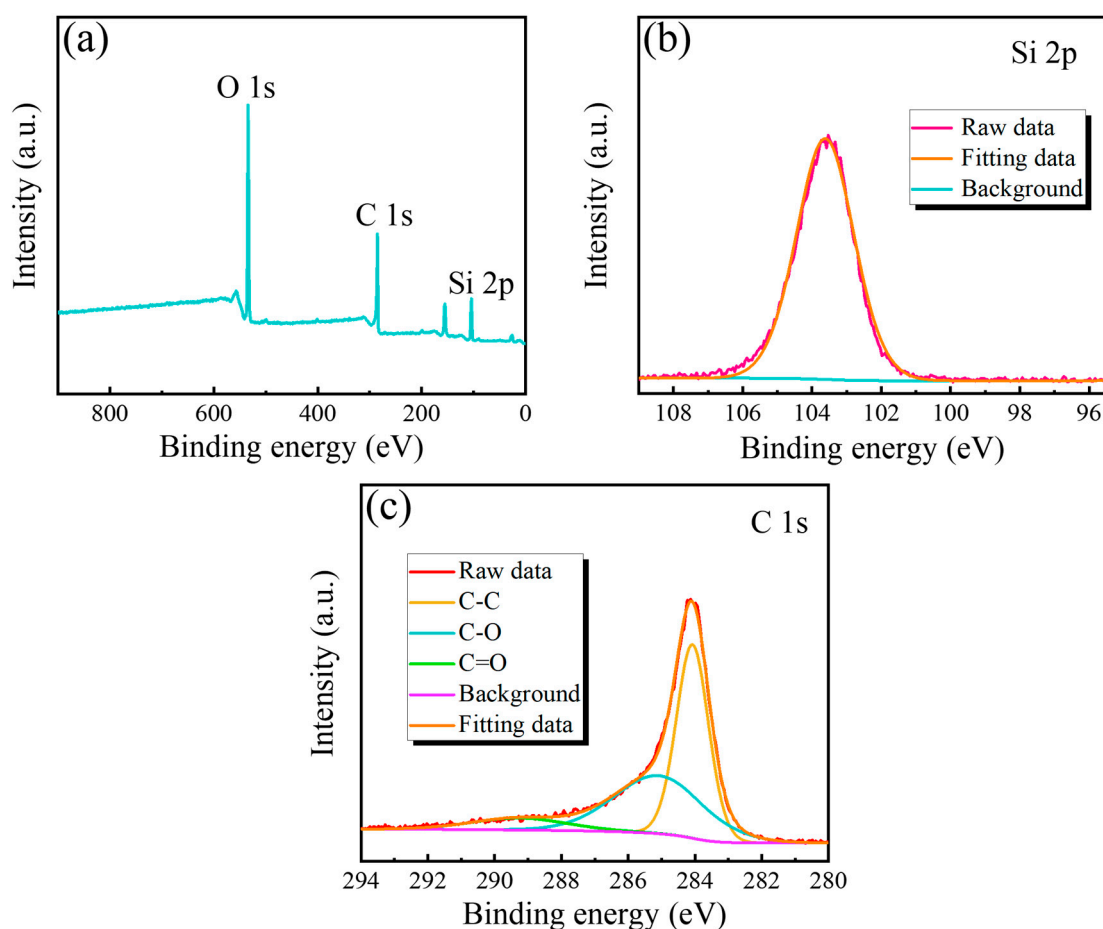


Figure 4. SiO₂@C-3: (a) XPS full spectrum, (b) Si 2p spectrum, (c) C 1s spectrum.

3.2. Electrochemical Properties

Figure 5a indicates the cycle performances of SiO₂-1, SiO₂-2, and SiO₂-3 at a current density of 0.2 A g⁻¹. As shown in Figure 5a, the initial discharge specific capacities of SiO₂-1, SiO₂-2, and SiO₂-3 are 549.4 mAh g⁻¹, 545.1 mAh g⁻¹, and 504.2 mAh g⁻¹, respectively. SiO₂-1 is superior to SiO₂-2 and SiO₂-3 in terms of the discharge specific capacity, displaying a high discharge specific capacity of 381.2 mAh g⁻¹ over 200 cycles. Additionally, SiO₂-1 is more stable than SiO₂-2 and SiO₂-3 during cycling. It can be seen that the wall thickness of SiO₂ nanotubes decreases with the decrease in reaction times, which shortens the Li⁺ diffusion distance and leads to better electrochemical performance.

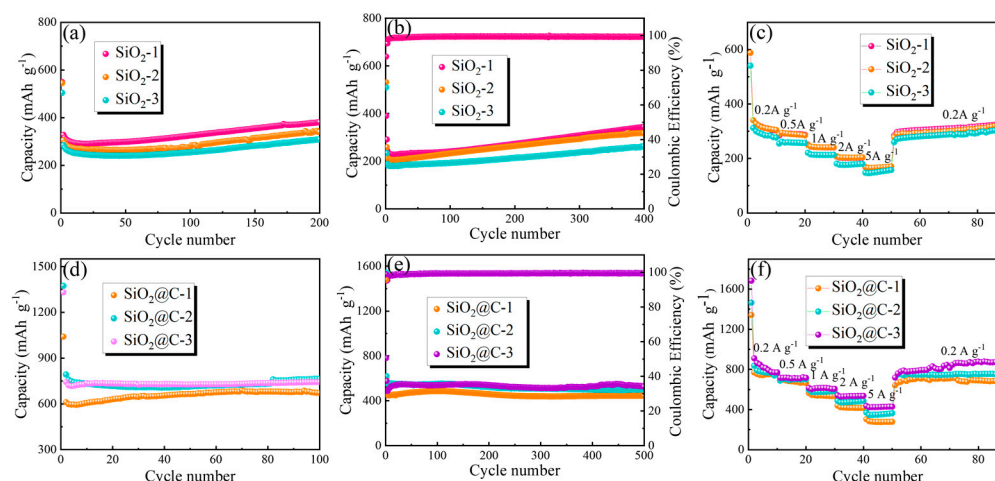


Figure 5. SiO_2 : (a) cycling performances at a current density of 0.2 A g^{-1} , (b) cycling performances at a current density of 1 A g^{-1} , and (c) rate performances. $\text{SiO}_2@\text{C}$: (d) cycling performances at a current density of 0.2 A g^{-1} , (e) cycling performances at a current density of 1 A g^{-1} , (f) rate performances.

Figure 5b demonstrates cycle performances of SiO_2 -1, SiO_2 -2, and SiO_2 -3 at a current density of 1 A g^{-1} . As can be shown, SiO_2 -1, SiO_2 -2, and SiO_2 -3 have initial discharge specific capacities of 639 mAh g^{-1} , 531 mAh g^{-1} , and 509 mAh g^{-1} , respectively. When cycled 400 times, discharge specific capacities of SiO_2 -1, SiO_2 -2, and SiO_2 -3 could reach 344.3 mAh g^{-1} , 317.5 mAh g^{-1} , and 263.4 mAh g^{-1} , respectively, with SiO_2 -1 maintaining the highest discharge specific capacity. In addition, from the second cycle onward, the coulombic efficiency of SiO_2 -1 is consistently above 95%. This demonstrates that SiO_2 with thinner walls performs better electrochemically than SiO_2 with thicker walls.

Figure 5c displays rate performances of SiO_2 -1, SiO_2 -2, and SiO_2 -3. Discharge specific capacities of SiO_2 -1, SiO_2 -2, and SiO_2 -3 are 587.6 mAh g^{-1} , 588 mAh g^{-1} , and 540.7 mAh g^{-1} at a current density of 0.2 A g^{-1} , respectively. At a current density of 5 A g^{-1} , SiO_2 -1, SiO_2 -2, and SiO_2 -3 have high discharge specific capacities of 171 mAh g^{-1} , 170.8 mAh g^{-1} , and 157.7 mAh g^{-1} , respectively. When the current density returns to 0.2 A g^{-1} , discharge specific capacities of SiO_2 -1, SiO_2 -2, and SiO_2 -3 stay at 310 mAh g^{-1} , 300 mAh g^{-1} , and 288 mAh g^{-1} , respectively. The electrochemical performance of SiO_2 with a thinner wall is better due to the fact that the thin wall helps to reduce the Li^+ diffusion distance.

Cycle performances of $\text{SiO}_2@\text{C}$ -1, $\text{SiO}_2@\text{C}$ -2, and $\text{SiO}_2@\text{C}$ -3 composites at a current density of 0.2 A g^{-1} are displayed in Figure 5d. After 100 cycles, discharge specific capacities of $\text{SiO}_2@\text{C}$ -1, $\text{SiO}_2@\text{C}$ -2, and $\text{SiO}_2@\text{C}$ -3 are 671.6 mAh g^{-1} , 743.2 mAh g^{-1} , and 743.2 mAh g^{-1} , respectively. As a whole, $\text{SiO}_2@\text{C}$ -3 has better cycle performance. All composites show good cycling stability, and $\text{SiO}_2@\text{C}$ composites have substantially higher discharge specific capacities than SiO_2 . Therefore, it is evident that carbon coating and nanotubular structure strengthen the structural stability and improve electrochemical performance.

Cycle performances of $\text{SiO}_2@\text{C}$ -1, $\text{SiO}_2@\text{C}$ -2, and $\text{SiO}_2@\text{C}$ -3 composites at a current density of 1 A g^{-1} are presented in Figure 5e. Discharge specific capacities all show a slight increase after the first few cycles. After 500 cycles, the discharge specific capacity of $\text{SiO}_2@\text{C}$ -3 (526.3 mAh g^{-1}) is significantly higher than those of $\text{SiO}_2@\text{C}$ -1 (446.4 mAh g^{-1}) and $\text{SiO}_2@\text{C}$ -2 (508.3 mAh g^{-1}), demonstrating that $\text{SiO}_2@\text{C}$ -3 has a better cycle performance compared with $\text{SiO}_2@\text{C}$ -1 and $\text{SiO}_2@\text{C}$ -2. In addition, the first coulombic efficiency of $\text{SiO}_2@\text{C}$ -3 is 50.52%, indicating that an irreversible Li^+ embedding process occurs during charge/discharge, but after the second cycle, the coulombic efficiency of $\text{SiO}_2@\text{C}$ -3 remains above 95%. The excellent cycle performance is related to its special structure and carbon coating. The results indicate that the amorphous carbon layer alleviates the volume change, and significantly enhances the structural integrity and cycle stability of $\text{SiO}_2@\text{C}$ composites during the lithiation/delithiation process. In addition, the carbon layer has a good electronic

conductivity, which provides the overall electronic conductivity of $\text{SiO}_2@\text{C}$. Additionally, a thicker carbon layer helps to improve the cycling stability, so the $\text{SiO}_2@\text{C}$ -3 composite shows the best electrochemical performance.

Figure 5f presents rate performances of $\text{SiO}_2@\text{C}$ -1, $\text{SiO}_2@\text{C}$ -2, and $\text{SiO}_2@\text{C}$ -3 composites at different current densities from 0.2 A g^{-1} to 5 A g^{-1} . As shown in Figure 5f, the discharge specific capacities of $\text{SiO}_2@\text{C}$ -1, $\text{SiO}_2@\text{C}$ -2, and $\text{SiO}_2@\text{C}$ -3 are $1342.1 \text{ mAh g}^{-1}$, $1464.2 \text{ mAh g}^{-1}$, and $1683.6 \text{ mAh g}^{-1}$ at a current density of 0.2 A g^{-1} , respectively. When the current density is up to 5 A g^{-1} , $\text{SiO}_2@\text{C}$ -1, $\text{SiO}_2@\text{C}$ -2, and $\text{SiO}_2@\text{C}$ -3 still have high discharge specific capacities of 304.2 mAh g^{-1} , 370.4 mAh g^{-1} , and 436.4 mAh g^{-1} . Furthermore, when the current density returns to 0.2 A g^{-1} , discharge specific capacities restore to 685 mAh g^{-1} , 745.9 mAh g^{-1} , and 870.4 mAh g^{-1} , exhibiting good rate performance. This further demonstrates that the thin wall thickness of SiO_2 can significantly decrease the Li^+ diffusion distance, and that the tubular structure has more space to effectively alleviate the volume expansion. At the same time, the amorphous carbon layer on the surface not only buffers the volume expansion during the charge/discharge process and improves the structural stability of the composite, but also improves the electrical conductivity of the material.

CV curves of $\text{SiO}_2@\text{C}$ -3 composites are presented in Figure 6a. There are three reduction peaks at the first CV cycle. In the case of a broad peak situated around 0.7 V , it may be caused by electrolyte decomposition and the formation of an SEI layer on the surface of the electrode [40]. In addition, the peak at 1.45 V may result from the reaction between SiO_2 and lithium [41]. These irreversible reactions lead to the formation of the SEI film, and consume a large amount of Li^+ , which may lead to a low initial coulombic efficiency and a large irreversible capacity. These peaks were not observed in the subsequent cycle, indicating that the SEI film has been almost completely generated [16,42]. The peak around 0 V may result from the alloying reaction between Si and lithium, which makes a contribution to lithium storage capacity [43]. It is observed that the oxidation peak appears at 0.2 V in the first charge process, and it may be assigned to the delithiation of the Li_xSi alloy [44]. At the subsequent cycle, CV profiles remain relatively stable, revealing that $\text{SiO}_2@\text{C}$ -3 has high electrochemical reversibility and good stability during the lithiation/delithiation process.

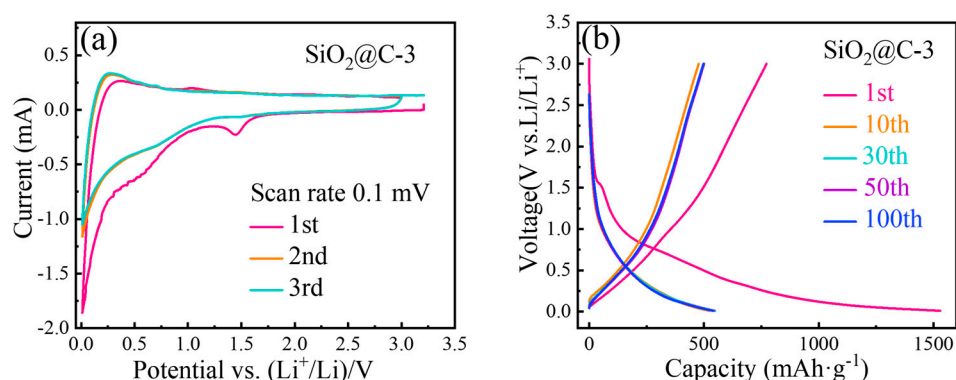


Figure 6. $\text{SiO}_2@\text{C}$ -3 composites: (a) CV curves, (b) charge and discharge performances.

Voltage profiles of $\text{SiO}_2@\text{C}$ -3 composites at a current density of 1 A g^{-1} are given in Figure 6b, which agree well with the CV measurements. It is shown that an irreversible lithiation reaction occurs at the first cycle, resulting in low coulombic efficiency. At subsequent cycles, voltage profiles do not change significantly, indicating that a more stable SEI film has been generated. It further demonstrates the benefit of the carbon layer to the cycling stability. It can be seen from the figure that the discharge specific capacity of $\text{SiO}_2@\text{C}$ -3 composites is 539.8 mAh g^{-1} after 100 cycles.

EIS tests further illustrate how carbon cladding modification improves electrochemical properties of SiO_2 . Figure 7a records an equivalent circuit used in the fitting plot, including R_s , R_{ct} , CPE1 , and W_s parameters. R_{ct} is the impedance during charge transfer and

W_s is partially related to the diffusion of Li^+ in electrode materials. Nyquist plots of SiO_2 and $\text{SiO}_2@\text{C}$ are displayed in Figure 7b, which indicate that all plots are made up of semicircles related to R_{ct} in the mid-high-frequency area and that diagonal lines are related to W_s in the low-frequency area [27]. In accordance with fitted results, the R_{ct} value of the $\text{SiO}_2@\text{C}$ -3 electrode ($220\ \Omega$) is significantly lower than those of the SiO_2 electrode ($279\ \Omega$), $\text{SiO}_2@\text{C}$ -1 electrode ($256\ \Omega$), and $\text{SiO}_2@\text{C}$ -2 electrode ($241\ \Omega$), suggesting that the amorphous carbon layer coated on the surface of SiO_2 nanotubes can effectively reduce the R_{ct} value. $\text{SiO}_2@\text{C}$ -3 has the smallest R_{ct} , indicating a faster charge transfer during the electrochemical reaction [45].

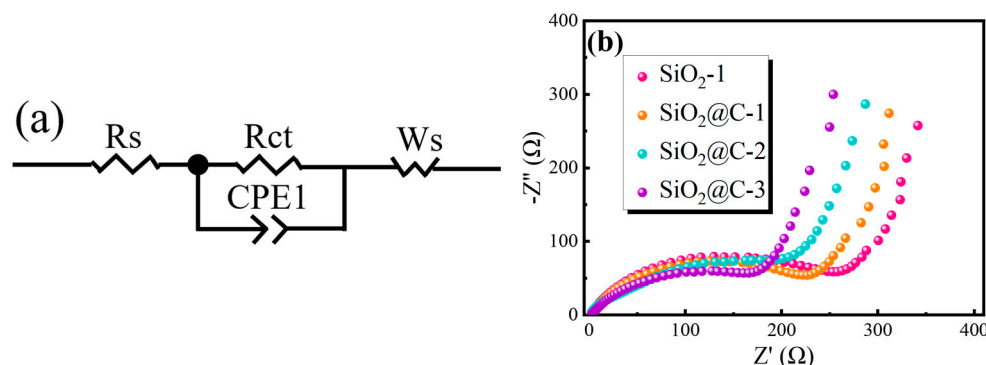


Figure 7. SiO_2 and $\text{SiO}_2@\text{C}$ composites: (a) equivalent circuit, (b) Nyquist plots.

Our work is compared with peers based on available data. Table 1 provides an overview of recent investigations on SiO_2 -based anode materials. Nanotubular $\text{SiO}_2@\text{C}$ is shown to have a larger discharge specific capacity and better stability. Better electrochemical properties of nanotubular $\text{SiO}_2@\text{C}$ anode materials may be explained by the synergistic effect of the tubular structure and carbon layer. In addition, the nanotubular structure with a wall thickness of only 11 nm reduces the Li^+ transport distance, and the hollow structure provides sufficient space to mitigate the volume expansion of nanotubular $\text{SiO}_2@\text{C}$ anode materials and improves the structural stability during the charging and discharging process. The carbon layer can provide additional electronic transport paths to improve electrical conductivity, and meanwhile acts as a support to relieve the mechanical stress generated during the lithiation/delithiation process. Beyond doubt, the $\text{SiO}_2@\text{C}$ composite can be further optimized to enhance properties.

Table 1. Previous works on silica-based anodes in recent years.

Materials	Active Material Loading (mg cm^{-2})	Current Density (A g^{-1})/Capacity (mAh g^{-1})/Cycle Number (n)	Current Density (A g^{-1})/Capacity (mAh g^{-1})/Cycle Number (n)	Ref.
$\text{SiO}_2@\text{C}$ composites	0.26–0.41	0.2/759.1/100	1/500/526.3	this work
SNTs@NC	-	0.1/781/200	-	[32]
SiO_2 nanotubes	-	0.04/232.5/100	-	[46]
$\text{SiO}_2/\text{C}@\text{SiO}_2@\text{CNT}$	1.0	0.1/644/200	1/5000/242	[47]
SiO_2/rGO	1.0	0.2/961/250	1/800/801	[48]
$\text{SiO}_2/\text{C}/\text{CNT}$ composites	0.87	0.05/502.3/100	1/315.7/1000	[49]

4. Conclusions

In this paper, nanotubular $\text{SiO}_2@\text{C}$ composites with controllable wall thicknesses were synthesized using ZnO nanorods as templates and glucose as carbon sources. The results reveal homogeneous and complete coating of the carbon layer on the surface of SiO_2 nanotubes. SiO_2 nanotubes with thin wall thicknesses alleviate the volume expansion

during cycling, which helps to avoid particles cracking or even crushing and improves the electrochemical performance. The carbon layer results in a perfect dispersion between SiO₂ nanotubes, providing a good conductive network for the composite and limiting the volume change and enhancing the structural stability. In addition, the nanotubular SiO₂@C composites exhibit exceptional performance, with a steady discharge specific capacity of 526.3 mAh g⁻¹ at a current density of 1 A g⁻¹ after 500 cycles. Moreover, they exhibit excellent rate performances, which maintain a discharge specific capacity of 420 mAh g⁻¹ even at a current density of 5A g⁻¹. This synthesis procedure is straightforward and simple, and it may also be utilized to prepare various materials.

Author Contributions: Conceptualization, X.H. and J.C.; methodology, X.H. and J.C.; validation, X.H. and J.C.; formal analysis, L.Z., Z.S. and G.Q.; investigation, T.G., C.S., G.L. and H.S.; resources, X.H. and J.C.; data curation, C.S. and T.G.; writing—original draft preparation, C.S., H.S., Z.S. and G.Q.; writing—review and editing, C.S., L.Z., X.H. and J.C.; visualization, C.S.; supervision, X.H. and J.C.; project administration, X.H. and J.C.; funding acquisition, X.H., J.C. and L.Z. All authors have read and agreed to the published version of the manuscript.

Funding: This work was supported by the National Natural Science Foundation of China (51764008), the Natural Science Research Project of Education Department of Guizhou Province (QJJ [2022]001), and the Science and Technology Plan of Guizhou Province (Qian KeHe [2021]-305).

Institutional Review Board Statement: Not applicable.

Data Availability Statement: Data supporting reporting results are available by request: hexm@tsinghua.edu.cn.

Conflicts of Interest: The authors declare no conflict of interest. Funders have no role in the design of the study; in the collection, analyses, or interpretation of data; in the writing of the manuscript; or in the decision to publish the result.

References

1. Dunn, B.; Kamath, H.; Tarascon, J.M. Electrical Energy Storage for the Grid: A Battery of Choices. *Science* **2011**, *334*, 928–935. [\[CrossRef\]](#)
2. McDowell, M.T.; Lee, S.W.; Nix, W.D.; Cui, Y. 25th Anniversary Article: Understanding the Lithiation of Silicon and Other Alloying Anodes for Lithium-Ion Batteries. *Adv. Mater.* **2013**, *25*, 4966–4985. [\[CrossRef\]](#) [\[PubMed\]](#)
3. Xia, S.B.; Yu, S.W.; Yao, L.F.; Li, F.S.; Li, X.; Cheng, F.X.; Shen, X.; Sun, C.K.; Guo, H.; Liu, J.J. Robust hexagonal nut-shaped titanium(IV) MOF with porous structure for ultra-high performance lithium storage. *Electrochim. Acta* **2019**, *296*, 746–754. [\[CrossRef\]](#)
4. Huang, G.Y.; Xu, S.M.; Xu, Z.H.; Sun, H.Y.; Li, L.Y. Core-Shell Ellipsoidal MnCo₂O₄ Anode with Micro-/Nano-Structure and Concentration Gradient for Lithium-Ion Batteries. *ACS Appl. Mater. Interfaces* **2014**, *6*, 21325–21334. [\[CrossRef\]](#)
5. Guo, T.; Luo, G.Y.; Shi, C.Y.; Shi, H.L.; Shi, Z.X.; He, B.F.; Chen, J.B. Thermal Burst Synthesis of High-Performance Si Nanotube Sheets for Lithium-Ion Batteries. *ACS Sustain. Chem. Eng.* **2022**, *10*, 4031–4039. [\[CrossRef\]](#)
6. Yoo, G.W.; Kim, C.; Jang, B.C.; Yang, S.B.; Son, J.T. Synthesis of Hollow Nanorods of SiO₂ Anode Material by AAO Template Synthesis Method for Lithium Ion Battery. *J. Nanosci. Nanotechnol.* **2015**, *15*, 8773–8776. [\[CrossRef\]](#) [\[PubMed\]](#)
7. Lener, G.; Otero, M.; Barraco, D.E.; Leiva, E.P.M. Energetics of silica lithiation and its applications to lithium ion batteries. *Electrochim. Acta* **2017**, *259*, 1053–1058. [\[CrossRef\]](#)
8. Li, W.; Wang, F.; Ma, M.N.; Zhou, J.S.; Liu, Y.W.; Chen, Y. Preparation of SiO₂ nanowire arrays as anode material with enhanced lithium storage performance. *RSC Adv.* **2018**, *8*, 33652–33658. [\[CrossRef\]](#) [\[PubMed\]](#)
9. Yang, X.Q.; Huang, H.; Li, Z.H.; Zhong, M.L.; Zhang, G.Q.; Wu, D.C. Preparation and lithium-storage performance of carbon/silica composite with a unique porous bicontinuous nanostructure. *Carbon* **2014**, *77*, 275–280. [\[CrossRef\]](#)
10. Takezawa, H.; Iwamoto, K.; Ito, S.; Yoshizawa, H. Electrochemical behaviors of nonstoichiometric silicon suboxides (SiO_x) film prepared by reactive evaporation for lithium rechargeable batteries. *J. Power Sources* **2013**, *244*, 149–157. [\[CrossRef\]](#)
11. Luo, F.; Li, X.C.; He, G.H.; Li, M.; Zhang, H.L. Preparation of Double-Shelled C/SiO₂ Hollow Spheres with Enhanced Adsorption Capacity. *Ind. Eng. Chem. Res.* **2015**, *54*, 641–648. [\[CrossRef\]](#)
12. Hou, X.H.; Zhang, M.; Wang, J.Y.; Hu, S.J.; Liu, X.; Shao, Z.P. High yield and low-cost ball milling synthesis of nano-flake Si@SiO₂ with small crystalline grains and abundant grain boundaries as a superior anode for Li-ion batteries. *J. Alloys Compd.* **2015**, *639*, 27–35. [\[CrossRef\]](#)
13. Chang, W.S.; Park, C.M.; Kim, J.H.; Kim, Y.U.; Jeong, G.; Sohn, H.J. Quartz (SiO₂): A new energy storage anode material for Li-ion batteries. *Energy Environ. Sci.* **2012**, *5*, 6895–6899. [\[CrossRef\]](#)

14. Dirican, M.; Lu, Y.; Fu, K.; Kizil, H.; Zhang, X.W. SiO₂-confined silicon/carbon nanofiber composites as an anode for lithium-ion batteries. *RSC Adv.* **2015**, *5*, 34744–34751. [\[CrossRef\]](#)
15. Liu, X.L.; Chen, Y.X.; Liu, H.B.; Liu, Z.Q. SiO₂@C hollow sphere anodes for lithium-ion batteries. *J. Mater. Sci. Technol.* **2016**, *33*, 239–245. [\[CrossRef\]](#)
16. Cao, X.; Chuan, X.Y.; Li, S.; Huang, D.B.; Cao, G.Z. Hollow Silica Spheres Embedded in a Porous Carbon Matrix and Its Superior Performance as the Anode for Lithium-Ion Batteries. *Part. Part. Syst. Char.* **2016**, *33*, 110–117. [\[CrossRef\]](#)
17. Chan, C.K.; Peng, H.L.; Liu, G.; McIlwrath, K.; Zhang, X.F.; Huggins, R.A.; Cui, Y. High-performance lithium battery anodes using silicon nanowires. *Nat. Nanotechnol.* **2008**, *3*, 31–35. [\[CrossRef\]](#)
18. Favors, Z.; Wang, W.; Bay, H.H.; George, A.; Ozkan, M.; Ozkan, C.S. Stable Cycling of SiO₂ Nanotubes as High-Performance Anodes for Lithium-Ion Batteries. *Sci. Rep.* **2014**, *4*, 4605. [\[CrossRef\]](#) [\[PubMed\]](#)
19. Ding, X.L.; Liang, D.W.; Zhao, H.D. Enhanced Electrochemical Performance Promoted by Tin in Silica Anode Materials for Stable and High-Capacity Lithium-Ion Batteries. *Materials* **2021**, *5*, 1071. [\[CrossRef\]](#)
20. Ding, X.L.; Liang, D.W.; Ai, X.; Zhao, H.D.; Zhao, N.; Chen, X.J.; Xu, J.H.; Yang, H. Synergistic Lithium Storage in Silica-Tin Composites Enables a Cycle-Stable and High-Capacity Anode for Lithium-Ion Batteries. *ACS Appl. Energy Mater.* **2021**, *4*, 2741–2750. [\[CrossRef\]](#)
21. Jia, D.L.; Wang, K.; Huang, J.G. Filter paper derived nanofibrous silica-carbon composite as anodic material with enhanced lithium storage performance. *Chem. Eng. J.* **2017**, *317*, 673–686. [\[CrossRef\]](#)
22. Wang, C.W.; Liu, K.W.; Chen, W.F.; Zhou, J.D.; Lin, H.P.; Hsu, C.H.; Kuo, P.L. Mesoporous SiO₂/carbon hollow spheres applied towards a high rate-performance Li-battery anode. *Inorg. Chem. Front.* **2016**, *3*, 1398–1405. [\[CrossRef\]](#)
23. Xiao, T.T.; Zhang, W.F.; Xu, T.; Wu, J.X.; Wei, M.D. Hollow SiO₂ microspheres coated with nitrogen doped carbon layer as an anode for high performance lithium-ion batteries. *Electrochim. Acta* **2019**, *306*, 106–112. [\[CrossRef\]](#)
24. Yuan, Z.N.; Zhao, N.Q.; Shi, C.S.; Liu, E.; He, C.N.; He, F. Synthesis of SiO₂/3D porous carbon composite as anode material with enhanced lithium storage performance. *Chem. Phys. Lett.* **2016**, *651*, 19–23. [\[CrossRef\]](#)
25. Guo, B.K.; Shu, J.; Wang, Z.X.; Yang, H.; Shi, L.H.; Liu, Y.N.; Chen, L.Q. Electrochemical reduction of nano-SiO₂ in hard carbon as anode material for lithium ion batteries. *Electrochem. Commun.* **2008**, *10*, 1876–1878. [\[CrossRef\]](#)
26. Lu, T.H.; Wang, H.; Wu, P.; Qu, M.T.; Si, L.; Tang, Y.W.; Zhou, Y.M. Highly Reversible and Fast Lithium Storage in Graphene Wrapped SiO₂ Nanotube Network. *Nanoscale* **2012**, *4*, 4002–4006. [\[CrossRef\]](#)
27. An, W.L.; Fu, J.J.; Su, J.J.; Wang, L.; Peng, X.; Wu, K.M.; Chen, Q.Y.; Bi, Y.J.; Gao, B.; Zhang, X.M. Mesoporous hollow nanospheres consisting of carbon coated silica nanoparticles for robust lithium-ion battery anodes. *J. Power Sources* **2017**, *345*, 227–236. [\[CrossRef\]](#)
28. Chen, Y.F.; Du, N.; Zhang, H.; Yang, D.R. Porous Si@C coaxial nanotubes: Layer-by-layer assembly on ZnO nanorod templates and application to lithium-ion batteries. *CrystEngComm* **2017**, *19*, 1220–1229. [\[CrossRef\]](#)
29. Zhang, B.; Jiang, Y.J. Improving the Flame Retardancy and Smoke Suppression of Poly(Lactic Acid) with a SiO₂@ammonium Molybdate Core-Shell Nanotubes. *Polym.-Plast. Technol. Eng.* **2019**, *58*, 843–853. [\[CrossRef\]](#)
30. Ren, Y.R.; Yang, B.; Wei, H.M.; Ding, J.N. Electrospun SiO₂/C composite fibers as durable anode materials for lithium ion batteries. *Solid State Ion.* **2016**, *292*, 27–31. [\[CrossRef\]](#)
31. Zheng, J.P.; Yu, Z.Z.; Wang, X.; Su, Q.; Shan, J.H. The effect of silica nanotubes on mechanical performance of polymethyl methacrylate nanocomposites: Comparison to spherical nano-silica. *J. Reinf. Plast. Compos.* **2015**, *34*, 1433–1443. [\[CrossRef\]](#)
32. Zhang, X.; Li, K.; Li, Y.B.; Liu, J.J.; Dai, J.T.; Li, Y.F.; Ai, F.R. Facile fabrication of SiO₂ nanotubes coated with nitrogen-doped carbon layers as high-performance anodes for lithium-ion batteries. *Ceram. Int.* **2020**, *47*, 1373–1380. [\[CrossRef\]](#)
33. Shao, D.; Tang, D.P.; Mai, Y.J.; Zhang, L.Z. Nanostructured silicon/porous carbon spherical composite as a high capacity anode for Li-ion batteries. *J. Mater. Chem. A* **2013**, *1*, 15068–15075. [\[CrossRef\]](#)
34. Agger, J.R.; Anderson, M.W.; Pemble, M.E.; Terasaki, O.; Nozue, Y. Growth of Quantum-Confined Indium Phosphide inside MCM-41. *J. Phys. Chem. B* **1998**, *102*, 3345–3353. [\[CrossRef\]](#)
35. Fan, W.G.; Gao, L. Synthesis of silicon dioxide hollow spheres assisted by ultrasound. *J. Colloid Interface Sci.* **2006**, *297*, 157–160. [\[CrossRef\]](#)
36. Alam, M.M.; Yamahana, H.; Bastakoti, B.P.; Luitel, H.N.; Zhao, W.W.; Yamauchi, Y.; Watari, T.; Noguchi, H.; Nakashima, K. Synthesis of hollow silica nanosphere with high accessible surface area and their hybridization with carbon matrix for drastic enhancement of electrochemical property. *Appl. Surf. Sci.* **2014**, *314*, 552–557. [\[CrossRef\]](#)
37. Liu, H.T.; Shan, Z.Q.; Huang, W.L.; Wang, D.D.; Lin, Z.J.; Cao, Z.J.; Chen, P.; Meng, S.X.; Chen, L. Self-Assembly of Silicon@Oxidized Mesocarbon Microbeads Encapsulated in Carbon as Anode Material for Lithium-Ion Batteries. *ACS Appl. Mater. Interfaces* **2018**, *10*, 4715–4725. [\[CrossRef\]](#)
38. Sen, P.N.; Thorpe, M.F. Phonons in AX₂ glasses: From molecular to band-like modes. *Phys. Rev. B* **1977**, *15*, 4030–4038. [\[CrossRef\]](#)
39. Ma, B.; Lu, B.; Luo, J.; Deng, X.; Wu, Z.; Wang, X. The hollow mesoporous silicon nanobox dually encapsulated by SnO₂/C as anode material of lithium ion battery. *Electrochim. Acta* **2018**, *288*, 61–70. [\[CrossRef\]](#)
40. Ma, X.M.; Wei, Z.P.; Han, H.J.; Wang, X.B.; Cui, K.Q.; Yang, L. Tunable construction of multi-shell hollow SiO₂ microspheres with hierarchically porous structure as high-performance anodes for lithium-ion batteries. *Chem. Eng. J.* **2017**, *323*, 252–259. [\[CrossRef\]](#)
41. Tang, C.J.; Liu, Y.N.; Xu, C.; Zhu, J.X.; Wei, X.J.; Zhou, L.; He, L.; Yang, W.; Mai, L.Q. Ultrafine Nickel-Nanoparticle-Enabled SiO₂ Hierarchical Hollow Spheres for High-Performance Lithium Storage. *Adv. Funct. Mater.* **2017**, *28*, 1704561. [\[CrossRef\]](#)

42. Liang, Y.H.; Chen, Y.M.; Ke, X.; Zhang, Z.X.; Wu, W.L.; Lin, G.D.; Zhou, Z.; Shi, Z.C. Coupling of Triporosity and Strong Au-Li Interaction to Enable Dendrite-Free Lithium Plating/Stripping for Long-Life Lithium Metal Anodes. *J. Mater. Chem. A* **2020**, *8*, 18094–18105. [[CrossRef](#)]
43. Li, M.; Li, J.H.; Li, K.; Zhao, Y.; Zhang, Y.G.; Gosselink, D.; Chen, P. SiO₂/Cu/polyacrylonitrile-C composite as anode material in lithium ion batteries. *J. Power Sources* **2013**, *240*, 659–666. [[CrossRef](#)]
44. Lu, B.; Ma, B.J.; Deng, X.L.; Wu, B.; Wu, Z.Y.; Luo, J.; Wang, X.Y.; Chen, G.R. Dual stabilized architecture of hollow Si@TiO₂@C nanospheres as anode of high-performance Li-ion battery. *Chem. Eng. J.* **2018**, *351*, 269–279. [[CrossRef](#)]
45. Liu, G.P.; Wang, N.; Qi, F.Y.; Lu, X.Y.; Liang, Y.H.; Sun, Z.P. Novel Ni-Ge-P anodes for lithium-ion batteries with enhanced reversibility and reduced redox potential. *Inorg. Chem. Front.* **2022**, *10*, 699–711. [[CrossRef](#)]
46. Tang, J.; Dai, X.Y.; Wu, F.Z.; Ma, Y.; Wang, X.; Jin, H.X.; Gu, Y.J.; Xie, Y.F. A simple and efficient one-pot synthesis of SiO₂ nanotubes with stable structure and controlled aspect ratios for anode materials of lithium-ion batteries. *Ionics* **2019**, *26*, 639–648. [[CrossRef](#)]
47. Wang, L.; Zhu, X.X.; Tu, K.K.; Liu, D.; Tang, H.L.; Li, J.S.; Li, X.; Xie, Z.Z.; Qu, D.Y. Synthesis of Carbon-SiO₂ hybrid layer@SiO₂@CNT coaxial nanotube and its application in lithium storage. *Electrochim. Acta* **2020**, *354*, 136726. [[CrossRef](#)]
48. Wang, K.X.; Zhu, X.D.; Hu, Y.J.; Qiu, S.Y.; Gu, L.L.; Wang, C.; Zuo, P.J. Stable anchoring and uniform distribution of SiO₂ nanotubes on reduced graphene oxide through electrostatic self-assembly for ultra-high lithium storage performance. *Carbon* **2020**, *167*, 835–842. [[CrossRef](#)]
49. Wang, S.Q.; Zhao, N.Q.; Shi, C.S.; Liu, E.Z.; He, C.N.; He, F.; Mam, L.Y. In-situ grown CNTs modified SiO₂/C composites as anode with improved cycling stability and rate capability for lithium storage. *Appl. Surf. Sci.* **2018**, *433*, 428–436. [[CrossRef](#)]

Disclaimer/Publisher's Note: The statements, opinions and data contained in all publications are solely those of the individual author(s) and contributor(s) and not of MDPI and/or the editor(s). MDPI and/or the editor(s) disclaim responsibility for any injury to people or property resulting from any ideas, methods, instructions or products referred to in the content.